ELSEVIER

Journal of Nuclear Materials 312 (2003) 1–9

journal of nuclear materials

www.elsevier.com/locate/jnucmat

Thermodynamic studies on $SrThO_3(s)$

R. Prasad *, Smruti Dash, S.C. Parida, Ziley Singh, V. Venugopal

Fuel Chemistry Division, Bhabha Atomic Research Centre, Mumbai 400085, India

Received 4 July 2001; accepted 10 June 2002

Abstract

The Gibbs energy of formation of $SrThO_3(s)$ has been determined using e.m.f. and manometric techniques. In the e.m.f. method, two fluoride cells have been constructed to determine $\Delta_f G^0_m(SrThO_3, s, T)$ using $CaF_2(s)$ as a solid electrolyte. The cells used are:

$$(-)O_2(g), Pt/SrO(s) + SrF_2(s)//CaF_2//(SrThO_3(s) + ThO_2(s) + SrF_2(s)/Pt, O_2(g)(+), \quad \text{(I)}$$

$$(-)O_2(g), Pt/SrThO_3(s) + SrF_2(s) + ThO_2(s)//CaF_2(s)//CaO(s) + CaF_2(s)/Pt, O_2(g)(+). \quad \text{(II)}$$

The observed e.m.f. values are represented by following respective expressions:

$$E\ (\mathrm{V}) \pm 0.0001 = 0.0998 + 3.254 \times 10^{-5} T\ (\mathrm{K}), \quad \text{(Cell I)}$$

$$E\ (\mathrm{V}) \pm 0.0001 = 0.0285 - 6.37 \times 10^{-5} T\ (\mathrm{K}). \quad \text{(Cell II)}$$

From the measured e.m.f. values of the cells and the $\Delta_f G^0_m(T)$ values from the literature, $\Delta_f G^0_m(SrThO_3, s, T)$ have been calculated and are respectively given as

$$\Delta_f G^0_m(SrThO_3, s, T) \pm 10\ \mathrm{kJ\,mol^{-1}} = -1829.2 + 0.2735T\ (\mathrm{K}) \quad (978 \leqslant T\ (\mathrm{K}) \leqslant 1154), \quad \text{(Cell I)}$$

$$\Delta_f G^0(SrThO_3, s, T) \pm 20\ \mathrm{kJ\,mol^{-1}} = -1853.5 + 0.2867T\ (\mathrm{K}) \quad (1008 \leqslant T\ (\mathrm{K}) \leqslant 1168). \quad \text{(Cell II)}$$

In the manometric technique, equilibrium $CO_2(g)$ pressures are measured over the three phase mixture: $\{SrThO_3(s) + SrCO_3(s) + ThO_2(s)\}$ using a mercury manometer from 1075 to 1197 K. The corresponding Gibbs energy as a function of temperature is given by

$$\Delta_f G^0_m(SrThO_3, s, T)(\mathrm{kJ\,mol^{-1}}) \pm 14 = -1865.4 + 0.3086T\ (\mathrm{K}).$$

1. Introduction

Thorium based nuclear fuels have been used in the early 1960 itself in nuclear reactors. Compared to uranium or plutonium based fuels, thorium based fuels offer a superior stability under irradiation, but the reprocessing of irradiated, thorium based fuel is more complicated due to high energy γ-radiation from the daughter products of U-232 [1]. Due to availability of uranium, and technological difficulties of the back end of thorium fuel cycle, interest on thorium based fuels has waned. However, in late 1990 there was a renewed interest in Europe and Russia in thorium as a carrier for burning excess plutonium in nuclear reactors [2]. The relative high abundance of thorium in India makes

* Corresponding author. Fax: +91-22 5505151.
E-mail address: fuelchem@magnum.barc.ernet.in (R. Prasad).

0022-3115/03/$ - see front matter © 2003 Published by Elsevier Science B.V.
PII: S0022-3115(02)00921-2

thorium fuel cycle attractive for Indian nuclear power programme. An advanced heavy water reactor (AHWR) is being developed at BARC, India with an aim of utilizing thorium for power generation [3,4]. It is self-sustaining in U-233. For smooth and safe operation of AHWR, it is important to examine the chemical reactions of the fuel matrix with fission products. Low-density compounds $SrThO_3(s)$ and $BaThO_3(s)$ might be formed in an operating AHWR due to the interaction of oxides of fission products barium and strontium with thoria fuel. These low-density compounds could be responsible for the swelling of the fuel pins. The thermodynamic stability of these compounds is important to predict their behavior in AHWR fuel. For this objective, we have carried out measurements to determine the $\Delta_f G^0_m(SrThO_3, s, T)$ values for these materials using e.m.f. and static manometric techniques.

2. Experimental

$SrThO_3(s)$ was prepared by the sol–gel method through citrate–nitrate gel combustion route. The compound obtained was identified as $SrThO_3(s)$ by X-ray diffraction (XRD) analysis. The X-ray pattern was taken on a Diano X-ray diffractometer using CuK_α radiations. The XRD pattern of the compound agreed well with that reported by Naray-Szabo [5] and Purohit et al. [6]. The observed XRD patterns for $SrThO_3(s)$ is given in Fig. 1. The XRD data of the compound could be indexed in a monoclinic unit cell with lattice parameters $a = 631.94$ pm, $b = 324.01$ pm, $c = 492.83$ pm and $\beta = 117.385°$.

Two separate three phase mixtures: $\{SrThO_3(s) + ThO_2(s) + SrF_2(s)\}$, $\{SrThO_3(s) + SrCO_3(s) + ThO_2(s)\}$ and two separate, two-phase mixtures: $\{SrO(s) + SrF_2(s)\}$, $\{CaO(s) + CaF_2(s)\}$ were prepared and made into separate pellets under a pressure of 10 MPa. These pellets were used for the e.m.f. and manometric measurements.

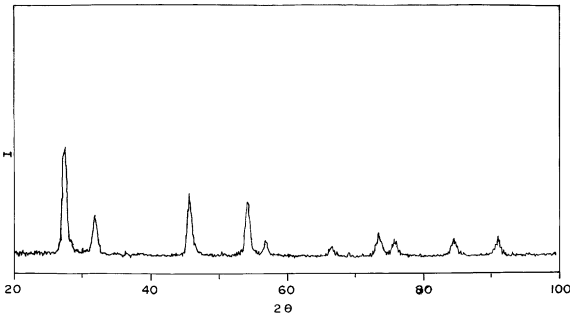

Fig. 1. The XRD pattern of $SrThO_3(s)$. Intensity (I) is plotted against 2θ.

2.1. E.m.f. technique

Solid fluoride electrolyte cell has been set up successfully in our laboratory for the study of Sr–Th–O system and is shown in Fig. 2. The defect structure of an ionic solid is responsible for the transport of anionic charge. F^- ion has the smallest size and lowest charge; fluorides can be expected to be good conductors. $CaF_2(s)$ electrolyte is used for measuring directly the high-temperature thermodynamic properties of compounds of highly electropositive metal like thorium. The investigation of thorium system with oxide electrolytes would be difficult on account of extremely low equilibrium oxygen pressures involved [7]. However, calcium fluoride electrolyte can be successfully used to measure meaningful e.m.f.s in Sr–Th–O system. The cells constructed for measurement of $\Delta_f G^0_m(SrThO_3, s, T)$ value were

$$(-)O_2(g), Pt/SrO(s) + SrF_2(s)//CaF_2//(SrThO_3(s) + ThO_2(s) + SrF_2(s)/Pt, O_2(g)(+), \quad \text{(Cell I)}$$

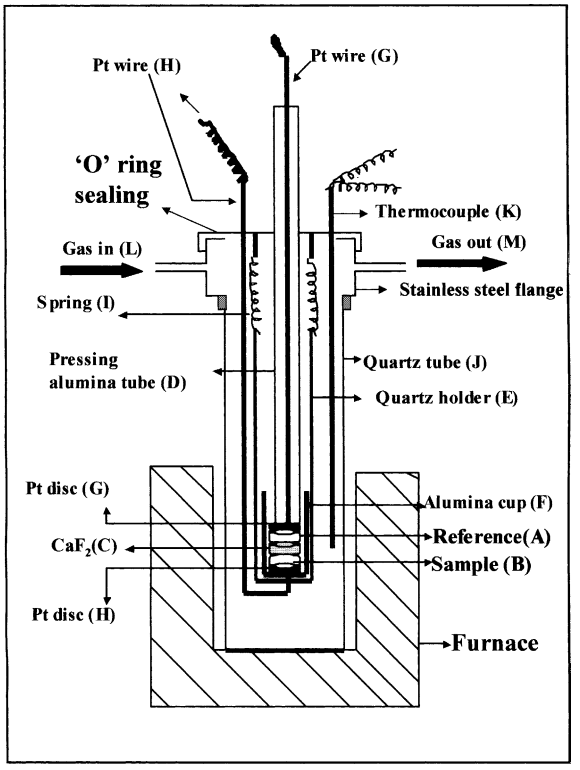

Fig. 2. Fluoride cell assembly. A: reference pellet, B: sample pellet, C: solid electrolyte (CaF_2), D: pressing alumina tube (hole at the bottom), E: quartz holder, F: alumina cup with hole at the centre, G: platinum wire with end platinum disc (above the electrolyte), H: platinum wire with end platinum disc (below the electrolyte), I: stainless steel spring, J: outer quartz tube, K: chromel alumel thermocouple, L: gas inlet and M: gas outlet.

$$(-)O_2(g), Pt/SrThO_3(s) + SrF_2(s) + ThO_2(s)$$
$$//CaF_2(s)//CaO(s) + CaF_2(s)/Pt, O_2(g)(+). \quad \text{(Cell II)}$$

$\{SrO(s) + SrF_2(s)\}$ and $\{CaO(s) + CaF_2(s)\}$ were used as reference electrodes (A) for cell (I) and (II) respectively. The three phase mixture: $\{SrThO_3(s) + ThO_2(s) + SrF_2(s)\}$ was used as sample electrode (B). $CaF_2(s)$ solid electrolyte (C) was used in the form of single crystal (10 mm dia and 3 mm thickness). High purity, low surface area and transparent, $CaF_2(s)$ single crystal was obtained from Solon Technologies, Inc., USA. The two parallel surfaces of this solid electrolyte were polished. The sample and reference electrodes were kept pressing against the two polished surface of the CaF_2 crystal by an alumina tube (D) and a quartz holder (E). It is a single compartment cell. Two electrodes (A & B) were placed on opposite surfaces of electrolyte CaF_2 (C) and were kept inside an alumina cup (F) with a hole at the centre. For electrical contact, electrodes were kept in contact with bottom platinum disc of the platinum wires (G & H). First platinum disc (G) was holding tightly on the outer bottom surface of the alumina tube (D) by taking out the Pt wire through bottom hole of the alumina tube (D). First electrode (A) was kept below this Pt disc (G). This electrode was pressed against the outer electrolyte (C) surface by means of alumina tube (D). Second Pt disc (H) was holding tightly on the inner surface of the alumina cup (F) by taking out the Pt wire through both the holes of the alumina cup (F) and quartz holder (E). The second electrode was kept on this Pt disc. This electrode was pressed against the inner surface of CaF_2 electrolyte by means of quartz holder (E). This quartz holder was held in position by three stainless steel springs (I) at the cold end of the cell. Good electrode contact was important for generation of thermodynamic data. To minimize contact problem, the interfacial contact was improved by using electrodes and electrolytes with pre-polished smooth surfaces and by using springs to hold the cell tightly together. The cell was housed in a quartz tube (J) using an O-ring seal. This arrangement had provisions for inserting thermocouple (K) for measuring cell temperature and for gas inlet (L) and out let (M). The two electrodes were flushed with high purity oxygen, free from hydrogen and moisture. The presence of moisture in the surrounding atmosphere can change the electrolytic properties of CaF_2. Water reacts with fluorides at high temperatures to produce HF(g). The hydrogen fluoride so produced attacks the cell container material and may also become a source of fluoride transfer from one electrode to other. Reaction of the electrolyte and/or electrode material with moisture may cause the growth of an insulating oxide layer which may subsequently affect the electrolyte–electrode contact or may modify the electrochemical reactions at the electrolyte–electrode interface, giving rise to mixed potentials. Hence, high purity oxygen gas (hydrogen less than 1 ppm, moisture less than 5 ppm) from the cylinder was allowed to pass through four successive traps (BTS catalyst (oxidized Cu based catalyst), silica gel, molecular shieves and magnesium perchlorate traps) for the removal of traces of $H_2(g)$ and $H_2O(g)$. Two electrodes and electrolyte were kept in the isothermal temperature zone of a Kanthal wire-wound furnace. Additionally a cylindrical stainless steel tube of 6 mm thickness and 120 mm length was placed in theconstant temperature zone of the furnace to further enhance the uniformity of the temperature in the zone. The cell temperature was controlled using a PID temperature controller. The stainless steel tube was grounded to avoid any AC pickup by e.m.f. signal. The cell temperature was measured using a pre-calibrated K-type thermocouple. The error in the temperature measurement was ± 1 K. The e.m.f. of the cell was measured using a high impedance Keithly model-614 electrometer.

The reversibility of electrolyte with reference and sample electrodes and absence of mixed potentials are important for the thermodynamic measurements. It was checked by passing a small current through the cells (I) and (II). The recorded e.m.f.s were decreased in the presence external current source and after removing it, e.m.f.s were back to the original value. The e.m.f.s of cells (I) and (II) were checked to be unaffected by time, temperature cycling, and gas flow rates and was reproducible from run to run. During the measurements, it was found that fluoride cell was sluggish in the operation. This might be due to the type of the oxide phase mixtures. Long equilibration time was required for single measurement. After the experiments XRD pattern of the sample and reference pallets were taken. No new peak was observed. This confirmed the absence of reaction between the electrode and the electrolyte.

2.2. Manometric method

This method was discussed in our earlier paper [8]. The equilibrium $CO_2(g)$ pressures over the three phase mixture $\{SrThO_3(s) + SrCO_3(s) + ThO_2(s)\}$ were measured using a mercury manometer. An all-metal ultra-high vacuum system was evacuated and tested for leak tightness for several days before actual pressure measurements. The three phase mixture was heated by a Kanthal wire-wound furnace and the temperature of the sample was measured by a pre-calibrated chromel–alumel thermocouple (± 1 K). The error in the measurement of pressure was (± 0.06 kPa). The $CO_2(g)$ over the three phase mixture $\{SrThO_3(s) + SrCO_3(s) + ThO_2(s)\}$ at constant temperature was measured using a manometer. The pressures were recorded as a function of temperature only at equilibrium.

3. Results

3.1. E.m.f. technique

Prior to the e.m.f. measurements, fluoride cell assembly (Fig. 2) has been standardized using $Fe(s) + FeF_2(s)$ and $Ni(s) + NiF_2(s)$ as reference and sample electrode, respectively. The standard cell can be given as

$$Pt, (Fe(s) + FeF_2(s))/CaF_2(s)/Ni(s) + NiF_2(s), Pt.$$

The e.m.f.s generated in this cell is due to the reaction:

$$NiF_2(s) + Fe(s) = FeF_2(s) + Ni(s). \quad (1)$$

E.m.f. values obtained from the cell are given in Table 1 and were expressed by a linear expression using the least square method as

$$E\ (\mathrm{V}) \pm 0.0005 = 0.3397 + 3.211 \times 10^{-5} T\ (\mathrm{K}). \quad (2)$$

The uncertainty quoted in reaction (2), is the standard deviation in the least squares fitting. The Gibbs free energy change of reaction (1) has been calculated from Eq. (2) and is given as

$$\Delta_r G^0(T) \pm 0.1\ \mathrm{kJ\,mol^{-1}} = -65.6 + 0.0062T\ (\mathrm{K}). \quad (3)$$

The $\Delta_f G^0(NiF_2, s, T)$ has been calculated using Eq. (3) and $\Delta_f G^0(FeF_2, s, T)$ from Belov and Trusov [9]. The $\Delta_f G^0(NiF_2, s, T)$ determined in this study matches excellently with that of literature [10]. This shows that the present e.m.f. cell assembly generates reliable thermodynamic data.

3.1.1. Cell (I)

In this cell, as $SrF_2(s)$ is more stable than $ThF_4(s)$, $SrF_2(s)$ with its coexisting SrO is taken as anode. In this particular case $SrF_2(s) + SrO(s)$ is more stable than $(SrThO_3(s) + ThO_2(s) + SrF_2(s))$. The fluorine potential in equilibrium with $(SrThO_3(s) + ThO_2(s) + SrF_2(s))$ is more than that of $(SrF_2(s) + SrO(s))$.

The cell reactions at anode and cathode can be given as

$$SrO(s) + 2F^- = SrF_2(s) + 1/2O_2(g) + 2e^-, \quad \text{(at anode)} \quad (4)$$

$$SrF_2(s) + ThO_2 + 1/2O_2(g) + 2e^- = SrThO_3(s) + 2F^-, \quad \text{(at cathode)} \quad (5)$$

The net cell reaction is

$$SrO(s) + ThO_2(s) = SrThO_3(s). \quad (6)$$

The overall cell reaction is a process of transfer of one mole of SrO(s) from the pure state (anode) to the heterogeneous mixture (cathode). E.m.f.s generated as a function of temperature are given in Table 2 and were fitted using least squares method and can be represented as

$$E\ (\mathrm{V}) \pm 0.0001 = 0.0998 + 3.254 \times 10^{-5} T\ (\mathrm{K}). \quad (7)$$

Computation of $\Delta_f G^0(SrThO_3, s, T)$ from Eq. (6) requires reliable Gibbs energy values for SrO(s) and $ThO_2(s)$. When reliable $\Delta_f G^0(T)$ values for required compounds are not available from a single source, more than one data sources have been used. Using the following Gibbs energy values from the literature [10,11]:

$$\Delta_f G^0(SrO, s, T) = -592.1 + 0.1020T\ (\mathrm{K}), \quad (8)$$

$$\Delta_f G^0(ThO_{2,}, s, T) = -1217.8 + 0.1778T\ (\mathrm{K}) \quad (9)$$

and e.m.f. values from Eq. (7), $\Delta_f G^0(SrThO_3, s, T)$ has been calculated and given as

Table 1
E.m.f. as a function of temperature for cell: $Pt/Fe(s) + FeF_2(s)//CaF_2//Ni(s) + NiF_2(s)/Pt$

T (K)	E (V)
880	0.3676
914	0.3697
967	0.3710
980	0.3708
991	0.3724
1002	0.3713
1006	0.3717
1012	0.3724
1017	0.3725
1032	0.3724
1042	0.3730
1096	0.3753

Table 2
E.m.f. as a function of temperature for cell (I): $(-)O_2(g), Pt/SrO(s) + SrF_2(s)//CaF_2//(SrThO_3(s) + ThO_2(s) + SrF_2(s)/Pt, O_2(g)(+)$ and for cell (II): $O_2(g), Pt/SrThO_3(s) + SrF_2(s) + ThO_2(s)//CaF_2(s)//CaO(s) + CaF_2(s)/Pt, O_2(g)(+)$

CELL (I)		CELL (II)	
T (K)	E (V)	T (K)	E (V)
978	0.1316	1008	0.0221
1005	0.1325	1038	0.0219
1026	0.1331	1045	0.0218
1028	0.1332	1066	0.0217
1055	0.1341	1077	0.0216
1082	0.1350	1098	0.0215
1109	0.1359	1114	0.0214
1127	0.1364	1120	0.0213
1130	0.1365	1143	0.0212
1149	0.1372	1168	0.0211
1154	0.1373		

$$\Delta_f G^0_m(SrThO_3, s, T) \pm 10\ kJ\,mol^{-1} = -1829.2 + 0.2735T\ (K) \quad (978 \leqslant T\ (K) \leqslant 1154). \tag{10}$$

3.1.2. Cell (II)

The fluorine potential over sample electrode: $(SrThO_3(s) + ThO_2(s) + SrF_2(s))$ is less than that over the reference electrode: $(CaF_2(s) + CaO(s))$. The cell reactions at anode and cathode can be given as

$$SrThO_3(s) + 2F^- = SrF_2(s) + ThO_2(s) + (1/2)O_2(g) + 2e^-, \quad \text{(at anode)} \tag{11}$$

$$CaF_2(s) + (1/2)O_2(g) + 2e^- = CaO(s) + 2F^-, \quad \text{(at cathode)} \tag{12}$$

and the net reaction is

$$CaF_2(s) + SrThO_3(s) = CaO(s) + SrF_2(s) + ThO_2(s). \tag{13}$$

E.m.f. values generated for the cell (II) are also given in Table 2. The e.m.f.s were least squares fitted with temperature and can be given by

$$E\ (V) \pm 0.0001 = 0.0285 - 6.37 \times 10^{-6} T\ (K). \tag{14}$$

Using the following $\Delta_f G^0(T)$ values from the literature [9–11],

$$\Delta_f G^0(SrF_2, s, T) = -1223.9 + 0.1648T\ (K), \tag{15}$$

$$\Delta_f G^0(CaO, s, T) = -638.6 + 0.1080T\ (K), \tag{16}$$

$$\Delta_f G^0(CaF_2, s, T) = -1221.3 + 0.1627T\ (K), \tag{17}$$

and that for $ThO_2(s)$ from Eq. (9) and e.m.f. values from Eq. (14), $\Delta_f G^0(SrThO_3, s, T)$ has been calculated and is given as

$$\Delta_f G^0(SrThO_3, s, T) \pm 20\ kJ/mol = -1853.5 + 0.2867T\ (K) \quad (1008 \leqslant T\ (K) \leqslant 1168). \tag{18}$$

The cell incorporating fluoride electrolyte has provided information on $\Delta_f G^0_m(SrThO_3, s, T)$ values in the lower temperature range, which cannot be conveniently investigated using other methods below 1000 K.

3.2. Equilibrium technique

The $CO_2(g)$ pressures were generated due to the following equation:

$$SrCO_3(s) + ThO_2(s) = SrThO_3(s) + CO_2(g). \tag{19}$$

Table 3
Equilibrium $CO_2(g)$ pressures at different temperatures over the three phase mixture: $\{SrThO_3(s) + SrCO_3(s) + ThO_2(s)\}$

T (K)	$p(CO_2, g)$ (kPa)
1075	3.1997
1089	4.2663
1109	6.2662
1131	9.9325
1159	14.1322
1185	20.5316
1197	23.1980

The variation of $p(CO_2, g)$ at various temperatures are given in Table 3 and can be represented by the following least square expression:

$$\ln p(CO_2, g)\ (kPa) \pm 0.001 = -20\,952/T\ (K) + 20.71. \tag{20}$$

The $\Delta_r G^0_m(T)$ for the reaction (19) can be given as

$$\Delta_r G^0_m(T) = -RT \ln p(CO_2, g) = \Delta_f G^0_m(SrThO_3, s, T) + \Delta_f G^0_m(CO_2, g, T) - \Delta_f G^0_m(ThO_2, s, T) - \Delta_f G^0_m(SrCO_3, s, T). \tag{21}$$

The values of $\Delta_r G^0_m(T)$ can be calculated from Eq. (21) and can be given as

$$\Delta_r G^0_m(T)\ (kJ\,mol^{-1}) \pm 0.3 = 174.2 - 0.1338T\ (K) \quad (1075 \leqslant T\ (K) \leqslant 1197). \tag{22}$$

The values of $\Delta_f G^0_m(SrThO_3, s, T)$ have been computed using Eq. (22) and $\Delta_f G^0_m(T)$ values for $ThO_2(s)$ from Eq. (9), $CO_2(g)$ and $SrCO_3(s)$ from following equation from the literature [10,11].

$$\Delta_f G^0(CO_2, g, T) \pm 5\ kJ\,mol^{-1} = -394.1 - 0.00084T\ (K), \tag{23}$$

$$\Delta_f G^0(SrCO_3, s, T) \pm 15\ kJ\,mol^{-1} = -1215.9 + 0.2638T\ (K). \tag{24}$$

The corresponding $\Delta_f G^0_m(SrThO_3, s, T)$ values can be given as

$$\Delta_f G^0_m(SrThO_3, s, T)\ (kJ\,mol^{-1}) \pm 14 = -1865.4 + 0.3086T\ (K) \quad (1075 \leqslant T\ (K) \leqslant 1197). \tag{25}$$

4. Discussion

The $\Delta_f G^0_m(SrThO_3, s, T)$ values determined from the two different techniques match reasonably. The

agreement of data from two different e.m.f. cells, is also good. In order to give a single $\Delta_f G^0_m(SrThO_3, s, T)$ expression, an average of the three equation has been taken and is given as

$$\Delta_f G^0_m(SrThO_3, s, T)\ (kJ\,mol^{-1}) \pm 14\ kJ\,mol^{-1} = -1849.4 + 0.2896T\ (K). \quad (26)$$

In the absence of thermal function data on $SrThO_3$(s) no attempt was made to get the corresponding enthalpy of formation value at 298.15 K from the present results.

Only one Gibbs energy value exists in literature by Ali et al. [12] to compare the present data. These authors [12] have determined $\Delta_f G^0_m(SrThO_3, s, T)$ values using Knudsen effusion forward collection technique [13] in the temperature range from 1670 to 2040 K and 2135 to 2420 K respectively for the reactions:

$$5SrThO_3(s) + W(s) = 5ThO_2(s) + Sr_2WO_5(s) + 3Sr(g), \quad (27)$$

$$4SrThO_3(s) + W(s) = 4ThO_2(s) + SrWO_4(s) + 3Sr(g). \quad (28)$$

The respective Gibbs energy values for $SrThO_3$(s) are

$$\Delta_f G^0_m(SrThO_3, s, T)\ (kJ\,mol^{-1}) \pm 4.1 = -1953.6 + 0.367T\ (K) \quad (1670 \leqslant T\ (K) \leqslant 2040), \quad (29)$$

$$\Delta_f G^0_m(SrThO_3, s, T)\ (kJ\,mol^{-1}) \pm 4.1 = -1960.0 + 0.369T\ (K) \quad (2135 \leqslant T\ (K) \leqslant 2420). \quad (30)$$

The $\Delta_f G^0_m(SrThO_3, s, T)$ values obtained by all the methods along with the additive oxide method are summarized in Table 4. In the additive oxide method, the $\Delta_f G^0_m(SrThO_3, s, T)$ has been calculated from the component oxide by simply adding $\Delta_f G^0_m(T)$ of SrO(s) and ThO_2(s) from Barin [10]. The Gibbs energy values obtained by different methods are compared at two different temperatures: $T = 1100$ and 1800 K in Table 4. The Gibbs energy values of the present study was found to be about 20 kJ mol^{-1} less negative at 1100 K and about 34 kJ mol^{-1} more negative at 1800 K than that of Ali et al. [12].

There is a controversy in the literature about the formation of $SrThO_3$(s) [14–16], though it is reported in the literature [5,6]. In the synthesis of the perovskites (AMO_3) compound from their constituent oxides, the entropy change is generally very small and the enthalpy change bears a linear relationship with the ionic radius of the six co-ordinate M ion [17]. Morss and Mensi [18] and William et al. [19] have found this relation for barium compounds. Goudiakas et al [20] have found that this linear relationship could be extended to analogous strontium compounds, especially those composed of cerium, terbium and americium, which exhibit a distorted perovskite structure. Fuger et al. [21] have estimated enthalpy of formation of actinide metal complex oxides with barium and strontium. The authors [21] have calculated that $SrMO_3$ compounds with actinides lighter than neptunium will not form, although the existence of these compounds M = Pa to Pu have been reported [22]. A useful parameter by which the stability of perovskites can be judged is the Goldschmidt tolerance factor [23]. The tolerance factor t represents the packing of spherical ions in perovskite. The value of t also describes the size of octahedral holes for accommodating the M^{+4} ions in the closed packed AO_3 layers. The ideal cubic structure where all ions are in contact has $t = 1$. The perovskite structures have been reported for AMO_3 compounds where tolerance factor lies between 1.0 and 0.8. The change in the molar volume also represents the relative packing efficiency of the ternary oxides. Morss and Eller [24] have found, positive molar volume for $BaMO_3$ type of compounds from the component oxides. The experimental $\Delta_f H^0_m(AMO_3, s, 298.15\ K)$ value from the component oxide $(AO(s) + MO_2(s) = AMO_3(s))$, for

Table 4
Comparison of $\Delta_f G^0_m(SrThO_3, s, T)$ values obtained by different methods with the literature value $\Delta_f G^0_m(SrThO_3, s, T)\ (kJ\,mol^{-1}) = A + BT\ (K)$

Authors	Methods	Temperature range (K)	$\Delta_f G^0_m\ (kJ\,mol^{-1}) = A + BT\ (K)$		$\Delta_f G^0_m$ (1100 K) (kJ mol^{-1})	$\Delta_f G^0_m$ (1800 K) (kJ mol^{-1})
			A	B		
Ali et al. [12]	Knudsen effusion					
	Eq. (29)	1670–2040	−1953.6	0.367	−1549.9	−1293.0
	Eq. (30)	2135–2420	−1960	0.369	−1554.1	−1295.8
Present work	(i) E.m.f. (CaF_2)					
	Cell (I)	978–1154	−1829.2	0.2735	−1528.4	−1336.9
	Cell (II)	1008–1168	−1853.5	0.2867	−1538.1	−1337.4
	(ii) Manometry	1075–1197	−1865.4	0.3086	−1525.9	−1309.9
	(iii) Calculation[a]	–			−1500.2	−1292.9

[a] Calculation = Sum of $\Delta_f G^0_m(SrO, s, T)$ and $\Delta_f G^0_m(ThO_2, s, T)$ [10].

Table 5
The structural and thermodynamic parameters for Perovskites compounds: $SrMO_3$ and $BaMO_3$, where M = Ti, Zr, Mo, Hf, Ce, Pr, Tb, Th, U, Np, Pu, Am and Cm

A	M^{4+} (Å)	$SrMO_3$(s)					$BaMO_3$(s)				
		t[a]	ΔV_m[b] (cm^3/mol)	ρ (gm/cm^3)	ΔH^0_m (298.15 K)[c] ($kJ\,mol^{-1}$) (estimated)	ΔH^0_m (298.15 K) ($kJ\,mol^{-1}$) (experimental)	t[a]	ΔV_m[b] (cm^3/mol)	ρ (gm/cm^3)	ΔH^0_m (298.15 K)[c] ($kJ\,mol^{-1}$) (estimated)	ΔH^0_m (298.15 K) ($kJ\,mol^{-1}$) (experimental)
Ti	0.605	0.910	−7.2	5.13	−102.8	-148.4 ± 511[d]	0.970	−8.8	5.77	−149.4	-161.2 ± 6[d]
Zr	0.72	0.861	−2.2	5.43	−64.8	-73.7 ± 3[e]	0.917	−3.9	6.21	−108.3	-125.2 ± 3[e]
Mo	0.65	0.890	−4.3	6.13	−87.3	-114.8 ± 5[f]	0.949	−6.9	7.08	−133.1	-129 ± 4[g]
Hf	0.71	0.865	−2.4	6.73	−67.9	-60.9 ± 2[h]	0.922	−4.9	7.55	−112.1	-103.4 ± 4[h]
Ce	0.87	0.804	2.0	5.77	−20.5	-7.4 ± 3.8[i]	0.857	0.8	6.36	−61.7	-49.5 ± 3.9[i]
Pr	0.85	0.811	–	–	−25.2	-49 ± 10[i]	0.864	0.1	6.46	−67.1	−147[i]
Tb	0.76	0.845	–	–	−52.3	-50.4 ± 2.1	0.900	–	–	−95.1	-89 ± 2.7[i]
Th	0.94	0.780	4.9	6.82	−1.9	-21.1 ± 5[j]	0.831	1.1	7.64	−41.5	-25.8 ± 10[k]
U	0.89	0.797	1.1	7.73	−15.1	-23.1 ± 11[i]	0.849	−0.6	8.28	−55.4	−57[i]
Np	0.87	0.804	–	–	−20.5	–	0.857	–	8.49	−61.7	–
Pu	0.86	0.807	0.9	8.03	−22.8	–	0.860	−0.2	8.47	−64.0	−51.8±[l]
Am	0.85	0.811	–	–	−25.9	-16.5 ± 4.1[i]	0.864	–	8.65	−67.1	-64.6 ± 3.4[i]
Cm	0.85	0.811	–	–	−25.9	–	0.864	–	–	−67.1	-58.8 ± 7.1[m]
Cf	0.821	0.821	–	–	−33.7	–	0.876	–	–	−76.4	-71.2 ± 5.6[m]

[a] Tolerance factor $t = (r_A + r_O)/(2^{1/2}(r_M + r_O))$, where r represents ionic radii (co-ordination number 6).
[b] For the reaction $AO(s) + MO_2(s) = AMO_3(s)$.
[c] Estimated from Eq. (31) for the reaction $AO(s) + MO_2(s) = AMO_3(s)$.
[d] From Ref. [32].
[e] From Ref. [29].
[f] From Ref. [31].
[g] From Ref. [30].
[h] From Ref. [17].
[i] From Ref. [20].
[j] From present work.
[k] Calculated in the present study from Ref. [28].
[l] From Refs. [24,33].
[m] From Ref. [21].

various AMO_3(s) have been fitted as a function of Goldschmidt tolerance factor by the present authors and is given as

$$\Delta_f H^0_m(AMO_3, s, 298.15\ K) \pm 19.4\ kJ\,mol^{-1} = 603.8 - 776.5t. \quad (31)$$

To correlate the structural and thermodynamic properties for the perovskites compounds of $SrMO_3$(s) and $BaMO_3$(s), tolerance factor, density, molar volume from the component oxide, have been calculated and are given in Table 5. Goldschmidt tolerance factor t has been calculated using ionic radii (co-ordination number 6) from Shannon [25]. The molar volume and density of the ternary oxides have been calculated from unit cell volume reported in the literature [26], whenever more than one unit cell volume was reported, the mean of several crystallographic determination have been taken. Molar volumes of the binary oxides have been taken from Belov and Trusov [9]. The experimental $\Delta_f H^0_m(AMO_3, s, 298.15\ K)$ from the component oxide have been calculated using the binary oxide data [10,11,27] as well as ternary oxide data [17,20,21,24,28–33] from the literature. These calculated values have also been included in the Table 5. The $\Delta_f H^0_m(AMO_3, s, 298.15\ K)$ values from component oxides have also been calculated from Eq. (31) and compared with that of experimental value in Table 5. It shows that compounds are thermodynamically stable even if structural parameters are not favorable. This table also shows that as M^{+4} ionic size increases (i) ΔV_m from component oxides become positive, (ii) tolerance factor decreases and (iii) $\Delta_f H^0_m(298.15\ K)$ from the component oxide decreases with a few exceptions. The decrease in $\Delta_f H_m(298.15\ K)$ and t could be due to large size of the actinide ions (M^{+4}) for six co-ordinated site in the ideal perovskite. The better fit of smaller ion in the M site can provide a driving force for oxidation of M^{+4} ion to either M^{+5} or M^{+6} ion. Thus, compounds having higher M^{+4} ionic radii could have lower $\Delta_f H^0_m(AMO_3, s, 298.15\ K)$ value from the component oxides. The Th^{+4} has higher ionic radii, thus it could form compounds with A ions with higher ionic radius. Hence, thorium compounds containing barium, are structurally more favorable than that of strontium

In order to resolve the ambiguity about the stability of $SrThO_3$(s), the $\Delta_f G^0_m(SrThO_3, s, T)$ values of Eqs. (10), (18), (25), (26), (29) and (30) and additive oxide values have been plotted with temperature in Fig. 3. Experimental Gibbs energy values are plotted in their measured temperature range and that for Eq. (26) and additive oxide values are plotted in the whole temperature range 900–2400 K. The difference in $\Delta_f G^0_m(SrThO_3, s, T)$ between the additive oxide method and our combined equation is $-31\ kJ\,mol^{-1}$ at 1100 K and $-35\ kJ\,mol^{-1}$ at 1800 K. The Gibbs energy change value for

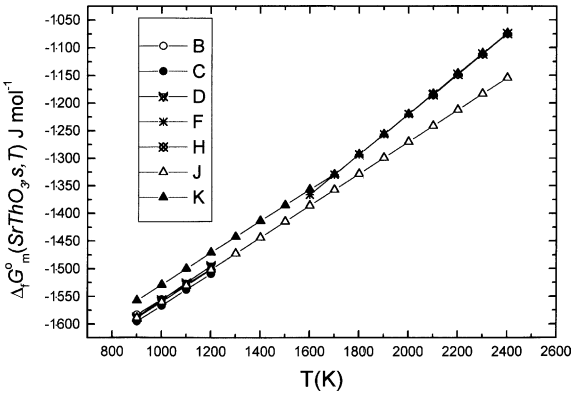

Fig. 3. Change in $\Delta_f G^0_m(SrThO_3, s, T)$ value with temperature. B: form Eq. (10), C: form Eq. (18), D: form Eq. (25), F: form Eq. (29), H: form Eq. (30), J: form Eq. (26) and K: form the component oxides.

the $SrThO_3$(s) from the component oxide, arrived in this study, reveals that $\Delta_f G^0_m(SrThO_3, s, T)$ has a marginal stability over its constituent oxides. It appears probable that the difficulties encountered in the literature [13–16] for the preparation of $SrThO_3$ might be due to the very refractory nature of ThO_2(s).

The experimentally derived thermodynamic properties of $SrThO_3$(s) suggest that the formation of strontium thorate from the constituent oxide is thermodynamically feasible at the normal working temperature of reactors based on thoria fuel. However, because of the marginal stability of $SrThO_3$(s), there is a possibility that strontium oxide will be fixed within the fuel pin by formation of a more stable strontium zirconate.

References

[1] P.G. Boczar, G.R. Dyck, J.D. Sullivan, R.J. Ellis, R.T. Jones, P. Taylor, A fresh look at thorium fuel cycles in CANDU reactors, Presented at IAEA Advisory Group Meeting on Thorium Fuel Cycle, Perspectives, 1997.
[2] H.T. Akie, T. Muromura, H. Takano, S. Matsuura, Nucl. Technol. 107 (1994) 182.
[3] A. Kakodkar, in: Indo-Russian seminar on Thorium Utilization, Obninsk, Russia, November 17–20, 1998.
[4] R. Chidambaram, in: M. Srinivasan, I. Kimura (Eds.), Proceedings of Indo-Japan Seminar on Thorium Utilization, Mumbai, India, December 10–13, 1990, p. 7.
[5] I. Naray-Szabo, Publ. Univ. Tech. Sci. Budapest 1 (1947) 30 (JCPDS-ICDD file no: 4-592).
[6] R.D. Purohit, A.K. Tyagi, M.D. Mathews, S. Saha, J. Nucl. Mater. 280 (2000) 51.
[7] E.C. Subbarao, Solid Electrolyte and Their Applications, Plenum, New York, 1980.
[8] S. Dash, Z. Singh, R. Prasad, D.D. Sood, J. Alloys Comp. 209 (1994) 193.
[9] G.V. Belov, B.G. Trusov, Computer-Aided Ref Book in Thermodynamical, Thermochemical and Thermophysical Properties of Species, 1983–1995, Moscow.

[10] I. Barin, Thermochemical Data of Pure Substance, 3rd Ed., VCH, Weinheim, 1995.
[11] M.W. Chase Jr. (Ed.), NIST JANAF Thermochemical Tables, 4th Ed., J. Phys. Chem. Ref. Data Monogr. 9 (1998).
[12] M. Ali, R. Mishra, S.R. Bharadwaj, A.S. Kerkar, S.R. Dharwadkar, D. Dash, J. Nucl. Mater. 299 (2001) 165–170.
[13] R.A. Rapp (Ed.), Techniques of Metals Research, vol. IV, part 1, Interscience Publishers, John Wiley & Sons, New York, 1970, p. 55.
[14] A. Hoffmann, Z. Phys. Chem. B 28 (1935) 65.
[15] R. Scholder, D. Rade, H. Schwarz, Z. Anorg. Allg. Chem. 362 (1968) 149.
[16] J. Fava, G. LeFlem, M. Devalette, L. Rabardel, J.P. Coutures, M. Foex, P. Hagenmuller, Rev. Int. Hautes. Temp. Refract. 8 (1971) 305.
[17] J. Huang, M. Yamawaki, K. Yamaguchi, M. Yasumoto, H. Sakarai, Y. Suzuki, J. Nucl. Mater. 247 (1997) 7.
[18] L.R. Morss, N. Mensi, in: McCarthy, G.J. Silber, H.B. Rhyne, J.J. Rhyne (Eds.), The Rare Earths in Modern Science and Technology, Plenum, New York, 1982, p. 279, 297.
[19] C.W. William, L.R. Morss, I.-K. Choi, in: G.S. Barney, I.D. Navratil, W.W. Schultz (Eds.), Geochemical Behavior of Disposed Radioactive Waste, ACS Symposium Series No. 264, American Chemical Society, Washington, DC, 1983, p. 323.
[20] J. Goudiakas, R.G. Haire, J. Fuger, J. Chem. Thermodyn. 22 (1990) 577.
[21] J. Fuger, R.G. Haire, J.R. Peterson, J. Alloys Comp. 200 (1993) 181.
[22] C. Keller, in: K.W. Bagnall (Ed.), MTP International Review of Science, vol. 7, Lanthanides and Actinides, Butterworths, London, 1972, p. 47.
[23] L.R. Goodenough, J.M. Lango, Landolt–Bornstein Tables, Group III, vol. 4a, Springer, Berlin, 1970, p. 47.
[24] L.R. Morss, P.G. Eller, Radiochim. Acta 47 (1989) 51.
[25] R.D. Shannon, Acta Crystallogr. A 32 (1976) 751.
[26] JCPDS International Centre for Diffraction data Version 2.11a, PDF-2 Data base, Swarthmore, PA, USA, 1987–1990.
[27] K.A. Gschneidner Jr., L. Eyring, G.R. Choppin, G.H. Lander (Eds.), Hand Book on Physics and Chemistry of Rare Earths, vol. 18, Lanthanides/actinides Chemistry, North Holland, Amsterdam, 1994, p. 491.
[28] R. Mishra, M. Ali (Basu), S.R. Bharadwaj, A.S. Kerkar, D. Das, S.R. Dharwadkar, J. Alloys Comp. 290 (1999) 97.
[29] S. Dash, D.D. Sood, R. Prasad, J. Nucl. Mater. 228 (1996) 83.
[30] S. Dash, Z. Sigh, R. Prasad, D.D. Sood, J. Nucl. Mater. 207 (1993) 350.
[31] S. Dash, Z. Sigh, R. Prasad, D.D. Sood, J. Alloys Comp. 201 (1993) 99.
[32] L.R. Reznitskii, A.S. Guzei, Russ. Chem. Review 47 (1978) 177.
[33] R.J. Fuger, H. Nitsche, P. Potter, M.H. Rand, J. Rydberg, K Spahiu, W.J. Ullman, P. Vitorge, H. Wanner (Eds.), Chemical Thermodynamics of Neptunium and Plutonium, Amsterdem, Elsevier, 2001.